VERY-LARGE-SCALE MOTIONS IN A TURBULENT CHANNEL FLOW

Jin Lee
Dept. of Mechanical Engineering
KAIST
Daejeon, 305-701, Korea
Lee.Jin@kaist.ac.kr

Jae Hwa Lee
Sch. for Engr. of Matter, Transport & Energy
Arizona State University
Tempe, AZ 85287-6106, USA
jhlee06@kaist.ac.kr

Jung-il Choi
Dept. of Computational Science and Engineering
Yonsei University
Seoul, 120-749, Korea
jic@yonsei.ac.kr

Hyung Jin Sung
Dept. of Mechanical Engineering
KAIST
Daejeon, 305-701, Korea
hjsung@kaist.ac.kr

ABSTRACT

Direct numerical simulation was carried out to investigate the spatial features of very large-scale motions (VLSMs) in a turbulent channel flow with $Re_\tau \approx 930$. Using the streak detection algorithm and the population trend, statistics of the spatial extents for both large-scale motions (LSMs) and VLSMs were obtained. This result showed that, at least one VLSM, on average, can be found in the wall-parallel $10\delta \times \delta$ plane (here δ is the channel half height), which provides a statistical evidence of the presence of VLSMs. Moreover, to clarify one of previous hypotheses regarding the formation of VLSMs, the upstream tracking of individual streaks was utilized for temporal analysis. The present study statistically supported that the connection of the upstream LSMs is mainly contributed to the formation of VLSMs; that is, the concatenation of the small structures to form VLSMs. The downstream tracking of VLSMs indicated that over than 30% of VLSMs survive for 9 wall-unit time. Finally, the spatial organization of LSMs and VLSMs was examined by the conditional averaging.

INTRODUCTION

Since Kim and Adrian (1999) first introduced the presence of very large-scale motions (VLSMs) in turbulent pipe flow, significance and influence of VLSMs on turbulent flow have been recognized by many researchers in various aspects so far. The presence of VLSMs in other flow types has been also observed; for instance, Monty et al. (2007) for channel flow and Lee and Sung (2011) for turbulent boundary layer (TBL). Although the role and existence of VLSMs are widely known, the formation mechanism of VLSMs is still in debate. One is explained by the concatenation of large-scale structures (Kim and Adrian, 1999; Guala et al., 2006) and the other is by the linear stability (McKeon and Sharma, 2010; Hellström et al., 2011). In particular, the instantaneous snapshots of multiple large-scale motions (LSMs) in a VLSM has been visualized by several studies. However, the visualization of the formation mechanism by instantaneous flow fields is limited to small number of snapshots, which conditionally sampled for the situation. A statistical approach is required to examine the formation mechanism with an appropriate criterion without loss of generality.

Recently, Kim (2012) summarised the existing question about VLSMs. Notwithstanding current interest on VLSMs, he addressed that there is still uncertainty whether the structures are originated from possible numerical or experimental artifact. For further investigation on VLSMs, there remains a need for clear solution for the generality of the presence. Opposite to the investigation on averaged flow field, that on the instantaneous flow field via statistical approach is necessary to provide clues for the generality and the creation of VLSMs. Dennis and Nickels (2011) (one of T. Nickelss posthumous work) used statistical investigation on VLSMs, and showed that the low-speed streaks were generally observed up to 7δ in the streamwise direction. Unfortunately, they used Taylors hypothesis which may make overestimation of the streamwise extent via disregarding diffusion. To give undisputed evidence, statistical investigation using pure 3D DNS dataset with large streamwise domain is required.

The objective of the present study is, therefore, to find out the evidence for the existence and formation mechanism of VLSMs. By tracking LSMs and VLSMs, the spatial and temporal relationships between LSMs and VLSMs are investigated using the DNS dataset of turbulent channel flow. From the results, statistical evidence of the streamwise-aligned connection of LSMs inside VLSMs is scrutinized.

NUMERICAL DETAILS

To obtain 3D flow fields for very-long streamwise domain, we simulated a turbulent channel flow by direct numerical simulation (DNS). The Navier-Stokes equation and the continuity are used as the governing equations:

$$\frac{\partial \tilde{u}_i}{\partial t} + \frac{\partial}{\partial x_j}\tilde{u}_i\tilde{u}_j = -\frac{\partial \tilde{p}}{\partial x_i} + \frac{1}{Re}\frac{\partial}{\partial x_j}\frac{\partial \tilde{u}_i}{\partial x_j}, \qquad (1)$$

$$\frac{\partial \tilde{u}_i}{\partial x_i} = 0 \qquad (\tilde{u}_i = U_i + u_i). \tag{2}$$

Here all terms are normalized by the channel half height (δ) and the laminar centerline velocity (U_{CL}). The Reynolds number ($Re \equiv U_{CL}\delta/\nu$) is 28,000 (or $Re_\tau \approx 930$, normalized by the friction velocity u_τ and δ). In the present study, x, y and z denote the streamwise, wall-normal and spanwise directions, respectively. The governing equations are solved using the fully implicit decoupling method by Kim et al. (2002). All terms are discretized with the Crank-Nicolson method in time and the 2nd-order central difference scheme in space. Both temporal and spatial accuracy are preserved in 2nd-order after the discretization. Periodic boundary condition is applied in the x and z directions. No-slip boundary condition is used on the bottom and top walls.

For inspection of the very-long structures, sufficiently large streamwise domain is required to prevent artificial periodicity from combined effect of the domain size and the periodic boundary condition (Simens et al., 2009). Thus, in the present study, the domain size is set to $10\pi\delta(x) \times 2\delta(y) \times 3\pi\delta(z)$, which is similar to that of Hoyas and Jiménez (2006) except for the streamwise extent. Based on the staggered grid system, the flow fields were simulated in $4,993(x) \times 401(y) \times 2,497(z)$ (almost 5 billions) grid points. Uniform grid spacing was used in the wall-parallel (x and z) direction, while non-uniform grid was used in the wall-normal (y) direction. The spatial resolution is Δx^+=5.86, Δy^+_{min}=0.0287, Δy^+_{max}=7.31 and Δz^+=3.51.

For the present massive computation, message passing interface (MPI) combined with OpenMP, namely hybrid parallelization was adopted for parallel computing. The simulation was carried out using 1,536 cores on Tachyon II (SUN X6275) in KISTI. The time step is $0.002\delta/U_{CL}$, which corresponds to Δt^+=0.0618. Total averaging time is $220\delta/U_{CL}$, which corresponds to 7 times to sweep the whole domain of the bulk flow. Total 2,010 snapshots for the 3D flow fields have been saved with the time step $0.1\delta/U_{CL}$. As shown in figure 1, the profiles of mean streamwise velocity and Reynolds stresses are in good agreement with those of the dataset $\mathrm{Re}_\tau = 934$ of Hoyas and Jiménez (2006).

DETECTION ALGORITHM

For the detection of elongated structures in the present study, we used a similar method with that of Nolan and Zaki (2012). Unlike their original algorithm, the following steps have been performed for the present turbulent channel flow. Figure 2 shows an extraction procedure in the present study. From the instantaneous flow field of the streamwise velocity fluctuations u in Fig. 2(a), small-scale structure becomes eliminated by a Gaussian filter. Note that the filter was not applied in the streamwise direction to preserve the streamwise extent of the long structure. A long-wavelength-pass filter in the streamwise direction was utilized thereafter. The filter was used to extract the structures longer than 1δ as LSMs and above. This is the same criterion as the cutoff value of Mathis et al. (2009) for computation of the amplitude modulation. From these two steps, figure 2(b) finally represents the filtered u-field, $u_{\geq LSM}$, with a sample of an iso-surface for 9δ-long structure.

From the filtered image, characteristic lines have been extracted to reduce the volume before computation of statistics. While the previous study of Dennis and Nickels (2011)

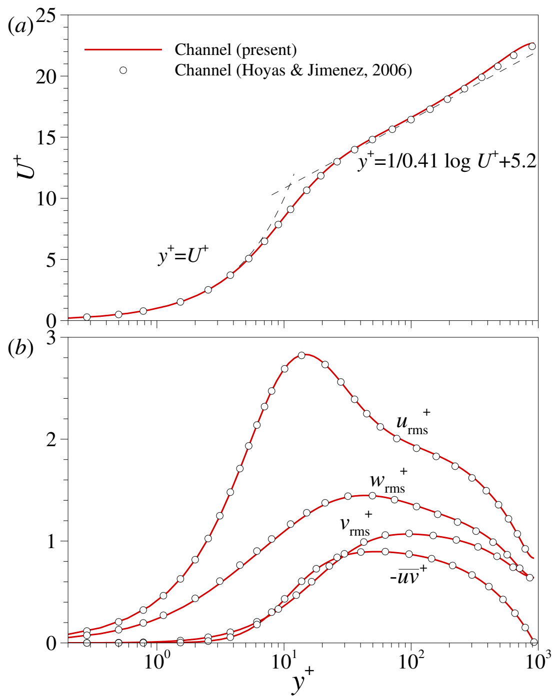

Figure 1. Turbulence statistics. (a) The mean streamwise velocity and (b) root-mean-square (rms) of turbulence intensities and the Reynolds shear stress normalized by the friction velocity.

determined the position of the characteristic line by center of an iso-surface (they called a 'spine'), the present study determines the position of the line by the local maximum of $|u|$. The spines obtained from the local maximum (hereafter C^{yz}, namely the core identified in the yz-plane)) is shown in figure 2(c). By comparison between 2(b) and (c), we found that C^{yz} represents the characteristic line of the packet. The C^{yz} streak longer than 1δ is regarded as LSMs hereafter. In the meantime, the same structures are also detected in the wall-parallel plane. For each wall-parallel plane of the filtered field in Fig. 2(b), the location of the local maximum of $|u|$ in the spanwise direction (hereafter C^{xz}, the core identified in the xz-plane) has been identified in Fig. 2(d). Earlier, the bound of the streamwise extent of VLSMs had been considered as 3δ-long by other researches (Guala et al. (2006), Dennis and Nickels (2011) and so forth). In the present study, the C^{xz} streak longer than 3δ is regarded as VLSMs similarly.

STATISTICS OF THE SPATIAL EXTENT

Figure 3 shows the population density, i.e., the number of structures in unit volume, of spatial extent of C^{yz} (Fig. 2(c). Since our focus is placed on LSMs, the yz-cores longer than 1δ have been conditionally sampled. As shown in Fig. 3(a), the population density decreases with increasing the streamwise length (L^{yz}_x). The density of the low-speed structure (C^{yz}_{neg}) is larger than that of the high-speed one (C^{yz}_{pos}) in all ranges. Most of the streamwise lengths are distributed less than 3δ; for example, the contribution of the density for the low-speed structure within 2δ and 3δ correspond to 77.3% and 94.8% of the total range, respectively. Since we supposed (C^{yz}_{neg} as the characteristic line of LSMs, this statistically supports that the streamwise length of LSMs can be considered as 3δ or shorter. This is in agreement with

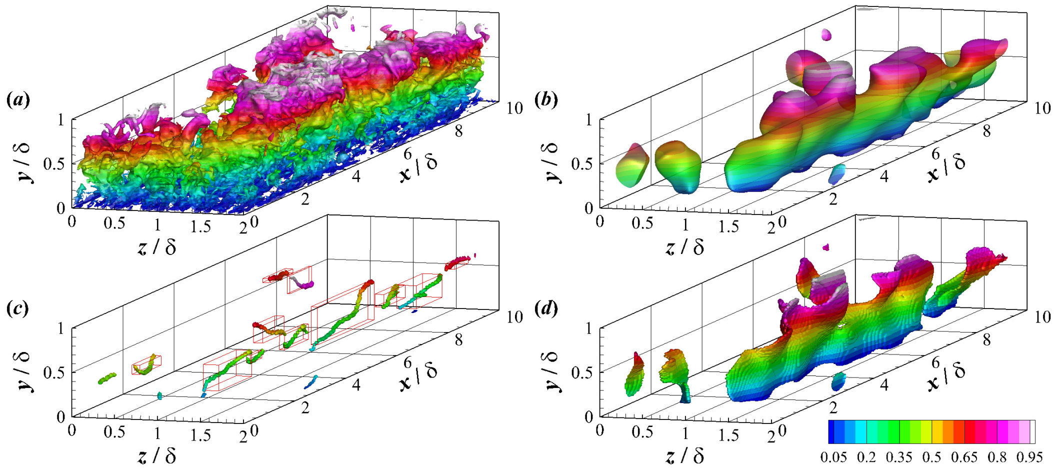

Figure 2. Iso-surfaces of (*a*) the streamwise velocity fluctuations, u, and (*b*) Gaussian and long-wavelength-pass filtered in the streamwise direction ($> 1\delta$) flow field, $u_{\geq LSM}$. Both are visualized by $u = -0.05U_{c,lam}$. Position of the local minimun in (*c*) the yz (cross-stream) plane and (*d*) the xz (wall-parallel) plane from the filtered image (*b*). Color indicates the wall-normal position normalized by the channel half-height δ. Red boxes in (*c*) indicate the minimal boxes including the cores. Note that only small domain is displyed for clarity.

the previous finding related to the extent of LSMs (Adrian et al., 2000).

Opposite to the distribution of the streamwise length, that of the wall-normal height shows a bell shape (Fig. 3(b)). In particular, the wall-normal extent of the core is mostly distributed near L_y^{yz}=0.16δ. From these results, the averaged inclination angle of C_{neg}^{yz} results in $\tan^{-1}\left(\frac{0.16\delta}{1.0\delta}\right)$=9.09°. The most probable angle in the present study is qualitatively consistent with the angle in the boundary layer flow of Adrian et al. (2000). Therefore, these results imply that C_{neg}^{yz} from the present detection method stands for the characteristic of LSMs.

Figure 4 displays statistics of the spatial extent of C_{neg}^{xz} (Fig. 2(d)) in the wall-parallel plane, where the subscript *neg* indicates the structures indentified by the negative u. The contour level indicates the population density of the streamwise length of the low-speed streak normalized by unit area. Figure 4(a) indicates 2D histogram of the density as a function of y and the streamwise lengh (L_x^{xz}). Even though most part of the distribution is biased toward the short length, very-long structures up to 20δ are detected near the wall. Practically, the density of the 3δ-long structures, denoted by the dotted line in Fig. 4(a), are 0.03 at $y = 0.15\delta$. This means that nine 3δ-long-streaks are observed in whole domain of the present simulation. To evaluate the universality of the present very-long structure, the cumulative density of all negative streaks for $L_x^{xz}/\delta > 3$ is shown in Fig. 4(b). The cumulative value at $y = 0.15\delta$ is 0.0984, which corresponds to 29 VLSMs in the present simulation. Thus, the observation of VLSM at the top of the log-layer is not rare and artificial but common in a turbulent channel flow. Even though the previous study of (Dennis and Nickels, 2011) has shown similar conclusion using Taylors hypothesis, which usually overestimates the streamwise length via neglecting change in the downstream, the present study clarifies a distribution of the length of VLSM from DNS dataset.

RELATIONSHIP BETWEEN LSM AND VLSM

Once the presence of VLSM is common, it naturally raises question how VLSM is formed. As mentioned in the introduction section, there have been two major hypotheses regarding to the origin of VLSM (Hellström et al., 2011). In vagueness of either side yet, it is necessary to determine whether one of them is still worth considering. Thus, in this subsection, relationship of the number of structures between LSM and VLSM will be statiscially examined via the present detection method. This can provide a basis whether the hypothesis of the streamwise-aligned LSMs (Guala et al., 2006) is plausible. For this reason, here we computed the number of crossing points between C_{neg}^{yz} and C_{neg}^{xz}, which indicates the number of LSMs inside VLSM at a certain wall-normal location. The ensemble-averaged number of LSMs (N_{cores}^{yz}) is defined in functions of the wall-normal position (y) and the streamwise length of VLSM (L_x^{xz}).

Figure 5 shows the distribution of most probable number of LSMs for each streamwise length of VLSM in the outer region. Here the xz-cores (C_{neg}^{xz}) which are longer than 3δ were considered only. Although the scattered symbols in figure 5 are not fully converged to a single line, the symbols show a roughly linear relation between the number of the yz-cores and the streamwise length of the xz-cores. This means that a single VLSM consists of several LSMs, and the number of LSMs is determined by the linear relation to the length of VLSM. This supports a statistical evidence of the hypothesis on the concatenation of LSMs (Kim and Adrian, 1999; Guala et al., 2006). Nonetheless this result cannot insist the concatenation of LSMs in terms of time evolution, the averaged number of LSMs is displayed participating the formation of VLSMs. However, to convince the concatenation of the formation mechanism, the assessment of temporal information on the streamwise-aligned LSMs is necessary.

In order to examine the origin of VLSM, we tracked the change in a shape of VLSM. For this analysis, individually identified VLSMs at reference time have been traced in the former three snapshots. The time duration for the tracking corresponds $\Delta t_{track}^{+} = 9.27$, which is 6 times larger than the Kolmogorov time scale. After the tracking, the individual

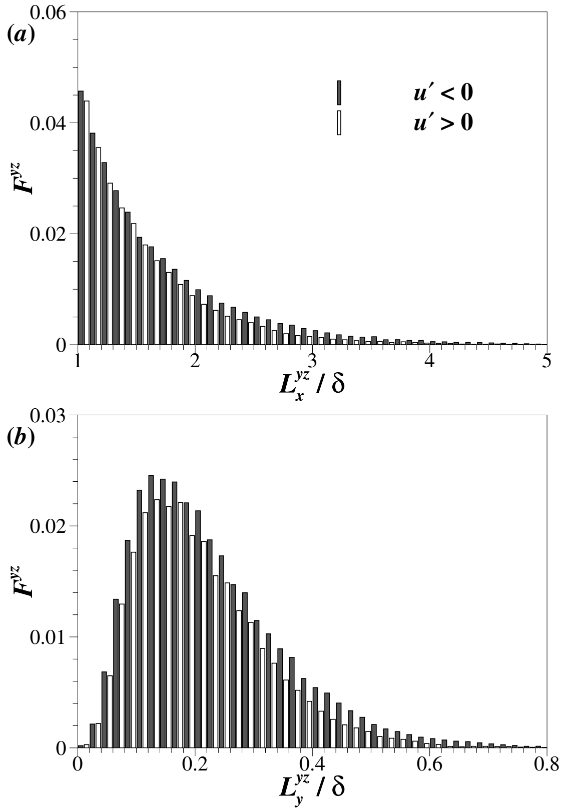

Figure 3. Histograms of observation frequency of (*a*) the streamwise length and (*b*) the wall-normal height of the *yz*-cores (C^{yz}) at y/δ=0.15, respectively. Both are normalized as unit volume ($\delta \times \delta \times \delta$). Red and blue bars indicate the *yz*-cores for the negative u (C^{yz}_{neg}) and the positive u (C^{yz}_{pos}), respectively. Note that cores longer than 1δ in x-direction have been conditionally sampled.

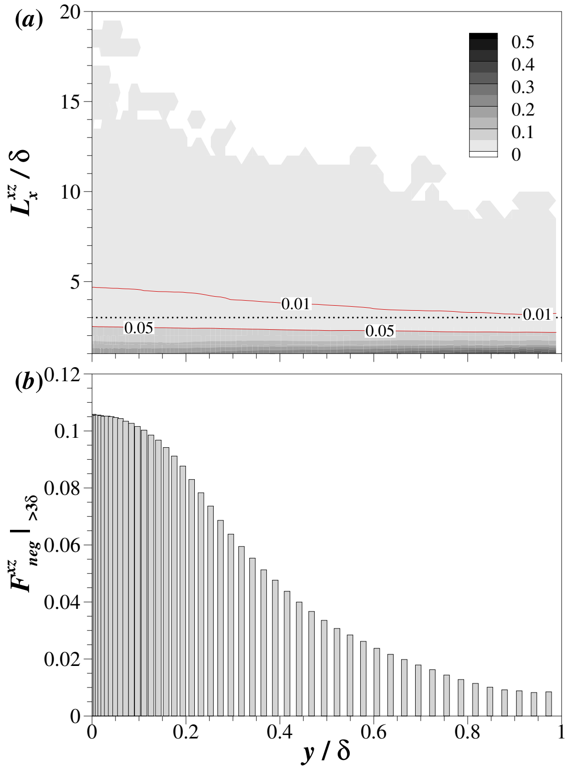

Figure 4. (*a*) 2-D histogram of observation frequency of the low-speed streak in the x–z plane (C^{xz}_{neg}). (*b*) 1-D histogram of observation frequency for 3δ-over ($L^{xz}_x/\delta > 3$ (above than dotted line in figure (*a*))) of the low-speed streak in the x–z plane. Both are normalized as unit x–z area ($\delta \times \delta$).

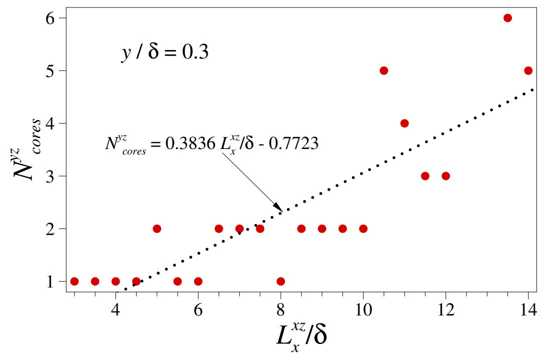

Figure 5. Distribution of the most probable number of the *yz*-cores (C^{yz}_{neg}) at $y/\delta = 0.3$ in a function of the streamwise length of the *xz*-cores (C^{xz}_{neg}), which indicates the number of LSMs in a function of the streamwise length of VLSM. A dotted line indicates the linear regression line.

VLSMs can be categorized in three types; first, the shape has been sustained as a single streak for Δt^+_{track} (namely “single”); second, the shape at the reference time has been made from several pieces of upstream (namely, “multiple”). We can consider this event as the VLSM has been formed by concatenation (or merging) of existing (just) long structures; Third, the single” and multiple” cases are mixed for Δt^+_{track}, which is denoted by uncertainty”. We can consider the single” and multiple” events as the VLSM has been formed by the growth of existing long structure and concatenation (or merging) of existing long structures, respectively. To quantify the contribution of these three types of VLSMs, the population density are shown in figure 6. Note that the sum of three types on the top of each bar in figure 6(a)) is exactly the same as that of figure 4(b). The contributions of each type for all VLSMs have similar proportion as shown in figure 6(a). The only difference is that the single” and the multiple” events have slightly large contributions near the wall and the core region, respectively. Since every structure longer than 3 has been used for this statistics, both the growth from shoter structure and the reduction from much longer structure are involved. When the sampling condition has been limited to the grown VLSMs from shorter structures with the critical length as 3δ (figure 6(b)), the “multiple” event turned out to be dominant. This result statistically supports that the connection of the upstream LSMs and small-scale motions (SSMs) is mainly contributed to the formation of VLSMs. Since the origin of the connection precess cannot be described from the statistics, the formation mechanism of VLSMs is still ambiguous. However, this result shows that the concatenation of the streamwise-aligned LSMs is plausible.

On the other hand, statistics of the present upstream tracking (figure 6(b)) is the same as that of the downstream tracking (not shown). Here the downstream tracking for the structure with the critical length (3δ) explains the extinc-

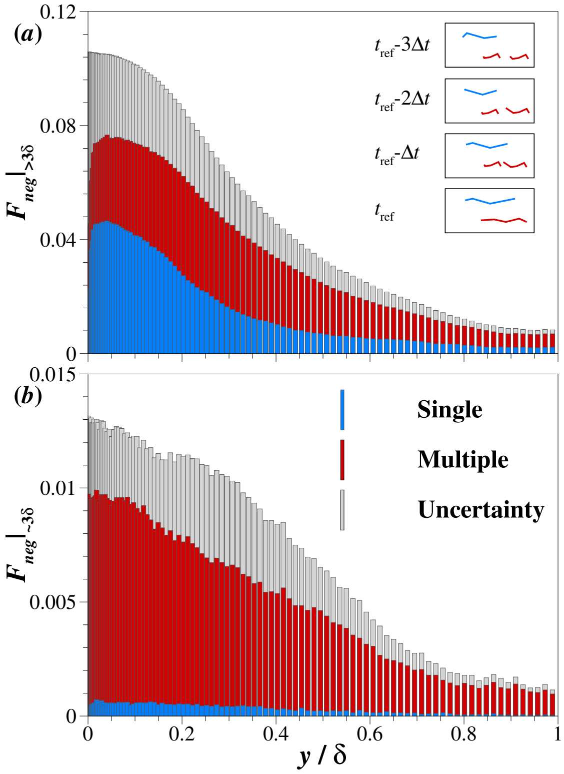

Figure 6. (a) Histogram of observation frequency for the structures longer than 3δ of the low-speed streak ($F_{neg}|_{>3\delta}$) in the x–z plane. (b) Histogram for conditionally sampled structures which newly become longer than 3δ from upstream short structures ($F_{neg}|_{\sim 3\delta}$). Both are normalized as unit x–z area ($\delta \times \delta$).

tion of VLSMs. Although it is natural that the sum of each type of the formation and extinction should be the same in a steady state, it is remarkable that the composition of these three types is also the same between the formation and extinction process. The inspection of the formation process of VLSMs may be beneficial to understand the extinction process of VLSMs and vice versa. On the other hand, figure 6 (a) indicates that the observation of VLSM is not only fugitive especially near the wall. Since the proportion of the single" event reaches over than one-third, a number of VLSMs retain their lengths within 3δ at least during Δt^+_{track}.

The relationship between LSM (identified by C^{yz}_{neg}) and VLSM (identified by C^{xz}_{neg}) has been examined as based on VLSM so far. Here, to convince the identical relationship from LSM, we computed conditionally averaged negative xz-cores around the negative yz-cores, i.e. $\langle C^{xz}_{neg}(r_x, y, r_z)|C^{yz}_{neg}(y_{ref})\rangle$, and showed in figure 7. Even though the contour level is low away from the reference location, the streamwise length between boundaries of positive and negative values (solid line) reaches 7δ. The spanwise spacing between the center of the positive and negative cores is shown approximately 0.5δ. Although the condition is defined from the LSM event, the result shows the very-long structures. This result indicates that the averaged flow structures around C^{yz}_{neg} are displayed as VLSMs. The present result corroborates that the spatial extents of LSMs are closely related with those of VLSMs. In particular, it is statistically supported that several LSMs are streamwisely aligned inside VLSMs, which is one of the hypothesis for the VLSM formation.

SUMMARY AND CONCLUSIONS

Direct numerical simulation was conducted to investigate the spatial features of very large-scale motions (VLSMs) in turublent channel flow with $Re_\tau \approx 930$. The computational domain was $10\pi\delta(x) \times 2\delta(y) \times 3\pi\delta(z)$, which is sufficient large to simulate VLSMs without Taylors hypothesis. The formation of VLSMs is statistically validated from the dataset. Using the streak detection algorithm and the population trend, the present study convinced that the observation of VLSMs is not only rare but common. Moreover, to clarify one of previous hypotheses regarding the formation of VLSMs, the upstream tracking of individual streaks was utilized for temporal analysis, which explains the contribution of the concatenation from large-scale motions (LSMs). The present study supported that the connection of the upstream LSMs is mainly contributed to the formation of VLSMs. This is consistent with Guala et al. (2006) which suggests the concatenation of several LSMs to form VLSMs. The result of the downstream tracking means that the observation of VLSMs is not only fugitive especially near the wall. However there is still uncertainty regarding the origin of arrangement of LSMs before the concatenation. The future work will therefore include the investigation of the internal mechanism.

This work was supported by the Creative Research Initiatives (No. 2013-003364) program of the National Research Foundation and was partially supported by KISTI under the Strategic Supercomputing Support Program.

REFERENCES

Adrian, R. J., Meinhart, C. D. & Tomkins, C. D. 2000 Vortex organization in the outer region of the turbulent boundary layer. *Journal of Fluid Mechanics* **422**, 1–54.

Buschmann, M. H. & Gad-el-Hak, M. 2010 Normal and cross-flow Reynolds stresses: differences between confined and semi-confined flows. *Experiments in Fluids* **49**, 213–223.

McKeon, B. J. & Sharma, A. S. 2010 A critical layer framework for turbulent pipe flow. *Journal of Fluid Mechanics* **658**, 336–382.

del Álamo, J. C., Jiménez, J., Zandonade, P. & Moser, R. D. 2004 Scaling of the energy spectra of turbulent channels. *Journal of Fluid Mechanics* **500**, 135–144.

Dennis, D. J. C. & Nickels, T. B. 2011 Experimental measurement of large-scale three-dimensional structures in a turbulent boundary layer. Part 2. Long structures. *Journal of Fluid Mechanics* **673**, 218–244.

Guala, M., Hommema, S. E. & Adrian, R. J. 2006 Large-scale and very-large-scale motions in turbulent pipe flow. *Journal of Fluid Mechanics* **554**, 521–542.

Hellström, L. H. O., Sinha, A. & Smits, A. J. 2011 Visualizing the very-large-scale motions in turbulent pipe flow. *Physics of Fluids* **23**, 011703.

Hoyas, S. & Jiménez, J. 2006 Scaling of the velocity fluctuations in turbulent channels up to Re_τ=2003. *Physics of Fluids* **18**, 011702.

Hutchins, N. & Marusic, I. 2007 Evidence of very long meandering features in the logarithmic region of turbulent boundary layers. *Journal of Fluid Mechanics* **579**, 1–28.

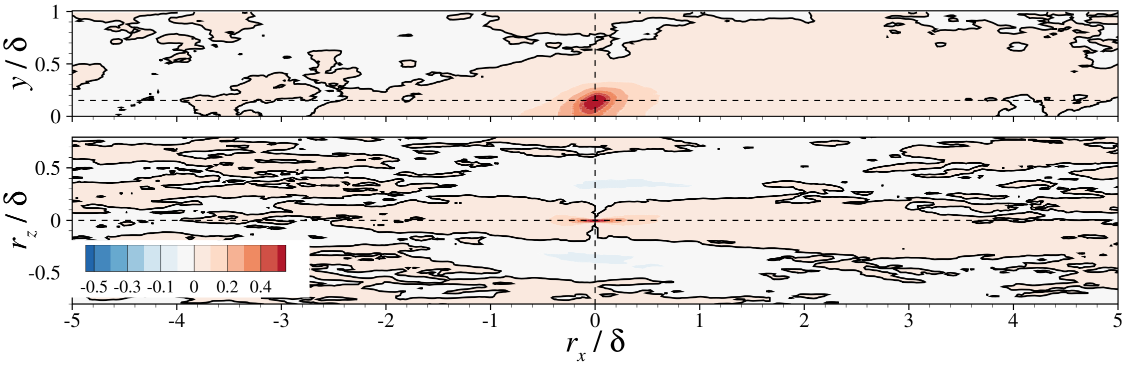

Figure 7. Side view (top) and top view (bottom) of conditionally averaged C^{xz}_{neg}-field around the negative yz-core $\langle C^{xz}_{neg}(r_x,y,r_z)|C^{yz}_{neg}(y_{ref})\rangle$. Here the reference wall-normal position y_{ref} is equal to 0.15δ (see dashed line). Solid line indicates the zero level.

Kim, J. 2012 Progress in pipe and channel flow turbulence, 1961–2011. *Journal of Turbulence* **13**(45), 1–19.

Kim, K. C. & Adrian, R. J. 1999 Very large-scale motion in the outer layer. *Physics of Fluids* **11**, 417–422.

Kim, K., Baek, S. J. & Sung, H. J. 2002 An implicit velocity decoupling procedure for the incompressible Navier-Stokes equations. *International Journal for Numerical Methods in Fluids* **38**, 125–138.

Lee, J. H. & Sung, H. J. 2011 Very-large-scale motions in a turbulent boundary layer. *Journal of Fluid Mechanics* **673**, 80–120.

Mathis, R., Hutchins, N. & Marusic, I. 2009 Large-scale amplitude modulation of the small-scale structures in turbulent boundary layers. *Journal of Fluid Mechanics* **628**, 311–337.

Monty, J. P., Stewart, J. A., Williams, R. C. & Chong, M. S. 2007 Large-scale features in turbulent pipe and channel flows. *Journal of Fluid Mechanics* **589**, 147–156.

Nolan, K. P. & Zaki, T. A. 2012 Conditional sampling and statistical analysis of transitional flows. In *Proceedings of the Summer Program 2012, Center for Turbulence Research, Stanford Univ.*, pp. 25–34.

Simens, M. P., Jiménez, J., Hoyas, S. & Mizuno, Y. 2009 A high-resolution code for turbulent boundary layers. *Journal of Computational Physics* **228**, 4218–4231.